Invited Article: A novel calibration method for the JET real-time far infrared polarimeter and integration of polarimetry-based line-integrated density measurements for machine protection of a fusion plant

A. Boboc, B. Bieg, R. Felton, S. Dalley, and Yu. Kravtsov

Citation: Review of Scientific Instruments **86**, 091301 (2015);
View online: https://doi.org/10.1063/1.4929443
View Table of Contents: http://aip.scitation.org/toc/rsi/86/9
Published by the American Institute of Physics

Invited Article: A novel calibration method for the JET real-time far infrared polarimeter and integration of polarimetry-based line-integrated density measurements for machine protection of a fusion plant

A. Boboc,[1,2,a)] B. Bieg,[1,3] R. Felton,[1,2] S. Dalley,[1,2] and Yu. Kravtsov[1,3]
[1]*EUROfusion Consortium, JET, Culham Science Centre, Abingdon OX14 3DB, United Kingdom*
[2]*CCFE, Culham Science Centre, Abingdon OX14 3DB, United Kingdom*
[3]*Institute of Physics, Maritime University of Szczecin, Szczecin, Poland*

(Received 2 March 2015; accepted 26 July 2015; published online 10 September 2015)

In this paper, we present the work in the implementation of a new calibration for the JET real-time polarimeter based on the complex amplitude ratio technique and a new self-validation mechanism of data. This allowed easy integration of the polarimetry measurements into the JET plasma density control (gas feedback control) and as well as machine protection systems (neutral beam injection heating safety interlocks). The new addition was used successfully during 2014 JET Campaign and is envisaged that will operate routinely from 2015 campaign onwards in any plasma condition (including ITER relevant scenarios). This mode of operation elevated the importance of the polarimetry as a diagnostic tool in the view of future fusion experiments. [http://dx.doi.org/10.1063/1.4929443]

I. INTRODUCTION

The JET Far-Infrared (FIR) interferometer/polarimeter diagnostic is a laser-based instrument[1] used for measuring several plasma parameters: electron line-integrated density (LID) via interferometry[2] and Faraday rotation angle (FAR) and Cotton-Mouton (CM) angle via polarimetry.[3] There were many developments[4–6] in the last decade of this instrument to increase the reliability and enhance[7] the measurement capabilities.

To date, its use has been limited to a narrow area of experiments such as q-profile control or motional Stark effect diagnostic calibration. Recent developments on reconstruction of JET magnetic equilibria require measurements of Faraday rotation angle together with an automatic way to validate the data and with a time resolution in millisecond range. This was not possible to do with the original Computer Automated Measurement And Control (CAMAC)[8]-based infrastructure and since 2011 developments of the polarimeter have been focused on upgrading the real-time infrastructure based on the Performance Optimization with Enhanced RISC Performance Computing (PowerPC)[9] architecture.

The installation of JET's ITER-like wall has caused new types of diagnostic issues such as tungsten impurity influxes during plasma pulses that heavily affect FIR interferometry (signal loss for up to half second) but also other systems as well. At that stage, it became critical to assess if the line-integrated density measurements from polarimetry could be used for density control and machine protection even if the data quality and the error level were not the same as the one provided by the interferometer.

After a few years of development and testing during recent campaigns, we have implemented a new real-time calibration of polarimetry to output not only the Faraday rotation angle measurements but also measurements of line integrated density and advanced validation flags in real-time.

The paper is organised as follows: Section I contains a detailed description of the JET polarimeter including hardware, software, as well as calibration process; Section II is dedicated to the method of complex amplitude ratio[10] and evaluation of line-integrated measurements from polarimetry. Various measurements are analysed and discussed in Section III and the way these were integrated within JET machine protection systems and machine protection is explained in Section IV. The remainder of the paper is dedicated to the conclusion and proposed further developments.

II. JET REAL-TIME POLARIMETER

A. General description

The JET FIR diagnostics rely on using two types of far infrared lasers (terahertz region in frequency domain) with wavelengths of 195 μm (Deuterated cyanide (DCN) laser) and 119 μm (methanol laser) as at these wavelengths the high temperature plasmas are optically transparent. The current diagnostic configuration probes the plasma via eight channels, four vertical and four lateral, with a sensitivity of 3×10^{17} particle/m^2 for the line-integrated density and 0.05°-0.2° for the Faraday rotation angle measurements. The polarimetry side is implemented by using only the DCN laser as at this wavelength, the expected Faraday rotation angle is large (up to 70°). The time resolution of the polarimeter is 1 ms and 0.01–1.5 ms for the interferometer.

The diagnostic system consists of components located in three different major areas: laboratory, basement, and torus area as shown in Figure 1.

All the three areas are purged 24 h/day with very dry air at −60° dewpoint humidity level to minimise FIR beam losses by absorption.

a)Author to whom correspondence should be addressed. Electronic mail: Alexandru.Boboc@ccfe.ac.uk

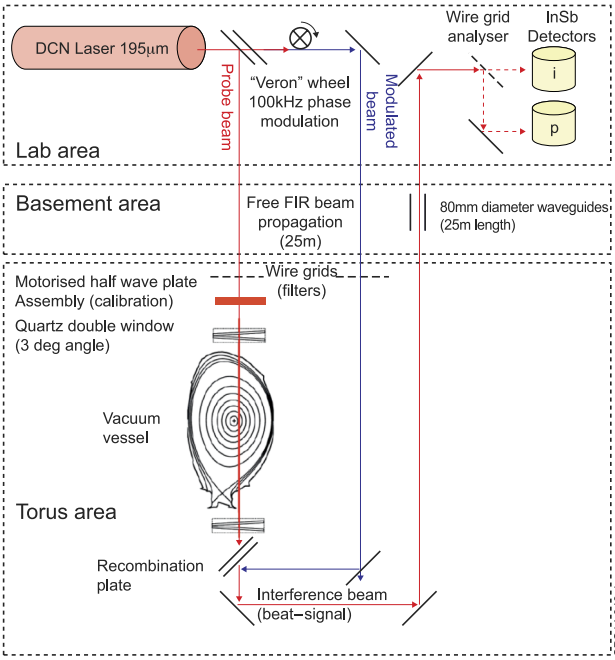

FIG. 1. Schematic representation of the JET FIR diagnostic system as used by the polarimeter.

The laboratory area contains the lasers with ancillary equipment; optical tables made of solid granite, cryogenic liquid helium cooled detectors systems, and electronics used for processing of the measurements.

The basement area consists of a large box 25 m long and cross section of about 1.5 by 2 m attached to the ceiling covering the space from the lab area to the bottom of the diagnostic tower located in the torus hall.

The torus hall area contains mainly the diagnostic tower. This is a 14 m high, 50 ton air-tight structure containing the input optics and recombination plates as well as the motorised half-wave plate (HWP) and associated opto-mechanical assemblies for the polarimetry calibration.

Nearly, all the optics can be moved remotely using pneumatic motors with the exception of the half-wave plates that are driven by standard electrical stepper motors.

The three areas are separated by 90 μm Polymethylpentene (TPX) pellicle windows that have the role of keeping the enclosures sealed but that act also as a safety barrier (critical during tritium experiments). These are also required to support the depression in the torus hall, a safety feature (nominally in the range of 200–250 Pa; more than 500 Pa during Deuterium-Tritium (D-T) campaign).

In terms of optical principle, the operation of the instrument is as follows: a linearly polarised laser beam is emitted by the DCN laser system. This is split in two components, one so-called probe signal that passes through the plasma and another one that is phase modulated with a Doppler wheel at a frequency of 100 kHz. After passing through the plasma, the probe beam becomes elliptically polarised with its polarisation plane rotated due to the Cotton-Mouton and Faraday effects, respectively, with respect to the initial polarisation state. The two beams (probe and modulated) are recombined at the recombination plate and the resulting interference beat-signal returns back to the laboratory where it is detected by the InSb cryogenic detectors (cooled at liquid helium temperature). From there, the signals are processed by the data acquisition system.

For each line of sight or channel, due to losses, the level of power that reaches the detectors is a few microwatts even if the original laser power is of the order of tens of milliwatt.

B. Short history

The polarimeter was originally designed in 1987 mainly for Faraday angle measurements. In 2001, new electronics were commissioned based on a real-time PowerPC architecture[9] technology for calculations of Faraday angle and q-profile for real-time control of the plasma[11] together with the implementation of real-time calibration on the CAMAC[8] system using novel half-wave plate rotators based on stepper motors (magnetically shielded) and remotely controlled by field-programmable gate array (FPGA)[12]-based cards. All the parameters are set remotely via software controlled by the JET Control and Data Acquisition System (CODAS).[13]

At a later stage (2004), the system was optimised to measure also the Cotton-Mouton[4] phase shift. In preparation for the 2008-2009 experimental campaigns, there was a requirement to set up the polarimeter for ITER-relevant high current plasma experiments (4.5-5 MA) and high density (90% of Greenwald limit). This is equivalent to a requirement to keep the error level below 0.2° for values of Faraday rotation angle of 70°-80°. This was at the limit of the existing electronics and the analog-to-digital converters (ADCs) were upgraded to 16 bits ADC for the real-time system.

In 2013, a novel calibration method based on complex amplitude ratio was implemented and tested extensively on a selection of 700 pulses covering 10 yrs of operation of the polarimeter system. A code written in Python was developed for automatic generation of the offline Processed Pulse Files (PPFs) database including automatic validation and integration with the reconstruction program EFIT++[14] recently deployed at JET. More recently, in September 2014, the real-time integration into the JET safety-system was completed, in particular, with the Plasma Density Validation (PDV) system that provides the density measurements for plasma gas injection feedback and control as well as the neutral beam injection safety interlocks.

C. Hardware description

Most implementations of polarimeters are for measuring Faraday rotation angle alone and therefore provide a calibration for this measurement. The most common way to implement this type of calibration is to use a HWP. This optical component rotates the polarisation plane corresponding to twice the angle between the optical axis and the input polarisation plane of a laser beam that traverses it. By comparing the mechanical rotation of the HWP with the detected laser signals, one can obtain the calibration curve for the actual Faraday rotation measurements in angular units.

The JET polarimeter uses this technique[5] and the main points of this are described schematically in Figure 2. The

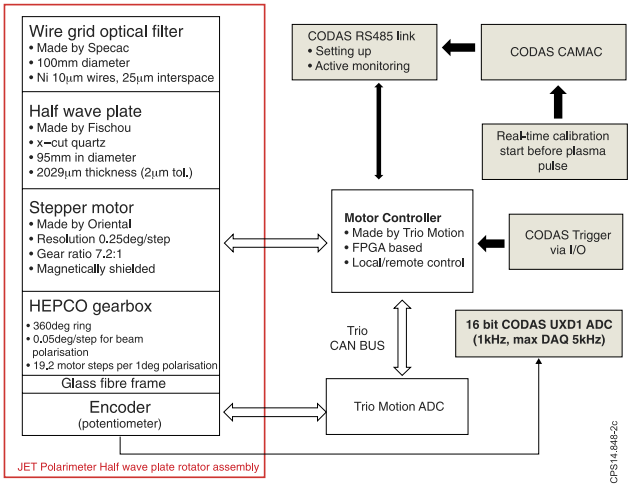

FIG. 2. The CAMAC-based JET polarimeter implementation.

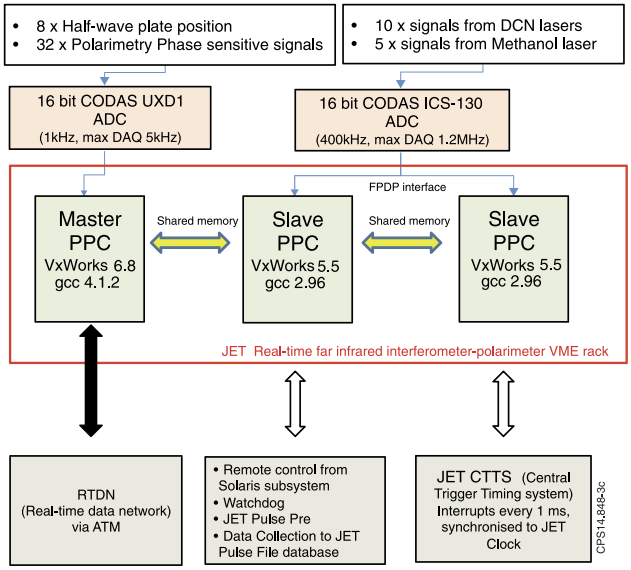

FIG. 3. JET Far Infrared (FIR) real-time interferometer-polarimeter implementation.

main part of the calibration hardware is the half-wave plate rotator assembly that contains a fixed wire grid used for optical filtering (it ensures the beam entering plasma is linearly polarised) a half-wave plate, a stepper motor, and a potentiometer linked with a high quality gearbox. All these components are installed on a fibreglass frame and fixed to the diagnostic tower. The assemblies are very close to the JET mechanical structure (50–100 cm depending on channel).

Communication to the half-wave plate assemblies is done via serial link and I/O from a CODAS CAMAC system that also is used for setting up and monitoring. Prior to a pulse, the diagnostic operator sets up the calibration range of the instrument. This depends mainly on the plasma current and maximum density for that pulse. These settings are sent via software to the motor controller that will move automatically the half-wave plate for the desired calibration range as well as returning back to the neutral position. In the current setup, this corresponds with a beam polarisation of 45° for the vertical channels to maximise Cotton-Mouton measurements[5] and 0° for lateral channels relative to the toroidal field direction.

D. PowerPC hardware

The real-time VME is based on PowerPC architecture and was developed in 2001 and upgraded over the years to have the final form as schematically represented in Figure 3. The most recent change was the operating system and the compiler on the master PPC as the new calibration software required implementation of new libraries able to deal with trigonometry functions on complex numbers, not normally provided for in the real-time PowerPC architecture at JET.

The analogue signals are currently acquired by ADC modules developed in-house by CODAS.[27] The system is synchronised with JET Composite Timing and Trigger System (CTTS)[27] and controlled remotely by daemon software that runs on a Solaris work station and via a dedicated Graphical User Interface (GUI) for setting up various parameters. Data acquisition is integrated within the JET Pulse File (JPF) database every pulse.

The real-time FIR interferometer/polarimeter signals are output to the JET Real-Time Data Network (RTDN)[27] via Asynchronous Transfer Mode (ATM) protocol.

E. Calibration logic

The automatic half-wave plate rotation required for an online calibration procedure was installed in 2002 but only recently was an algorithm implemented for real-time data analysis using the Complex Amplitude Ratio (CAR) method. This is described in Section II.

The time-flow of the calibration is depicted in the left part of Figure 4 and can be explained in a simplified form as follows: at the pulse start, the parameters corresponding to the calibration range for the polarimeter are sent to the motor controller at the initialisation phase prior the pulse.

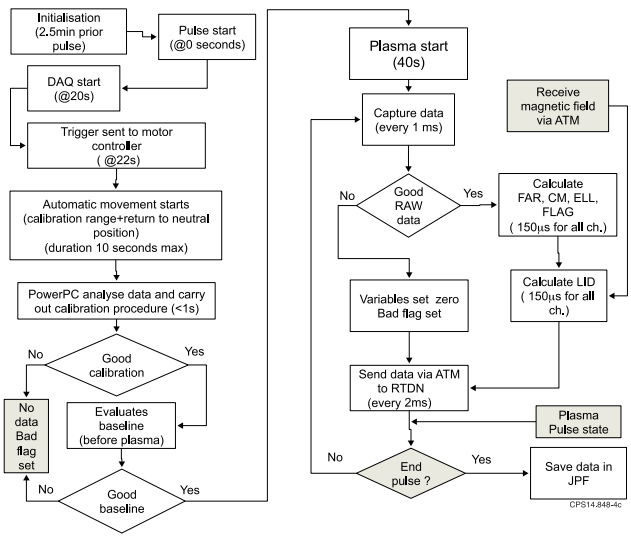

FIG. 4. Data acquisition procedure for one channel of JET polarimeter-calibration procedure is presented on the left.

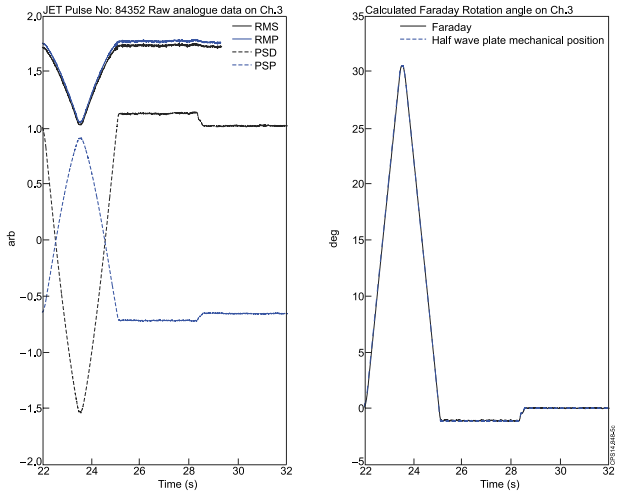

FIG. 5. Real-time raw signals in bits (left side) and calculated Faraday angle (FAR3) compared with mechanical HWP position (HWP3) in degrees for channel 3.

The calibration, with cycle of 10 s, is triggered 28 s plasma starts, process in which the half-wave plates ramp up and down according to calibration range. After that there are 5 s in which the calibration has to run for all channels after which the results can be applied in real-time to the input signals. During the actual plasma pulse (after 40 s), the calibration is applied and data are calculated, evaluated on every 1 ms cycle, and published via RTDN as shown in Figure 4.

More detailed information is displayed in Figure 5 where the raw data measured by the analogue phase-sensitive electronics during the process of calibration alone (see the definition of Eq. (9) of raw data) as well as the output of measurements for a JET pulse are pictured. In this particular example, the data are displayed from channel 3 that was set to cover a Faraday rotation angle range of 30° from an initial position of 45°. At 22 s in the pulse, a trigger is sent to the motor controller, and this automatically rotates the plate for the desired range (in this case 15° mechanical rotation of the HWP that corresponds to 30° of laser beam polarisation) and returns it to the neutral position of 45°. The system was designed to cover up to 90° of polarisation scan plus return to the neutral position scan in 10 s maximum.

III. CAR METHOD

A. Basic physics considerations

The principles of interferometry/polarimetry have been described in detail in several references.[3,4] Interpretation of the measurements from this type of device must take into account several properties of the plasma: refractive index, optical activity, and birefringence. Due to these three effects, linearly polarised electromagnetic radiation sent into a plasma can provide three measurements:

- *Interferometry phase shift* of the probe beam proportional to the plasma electron LID.
- *FAR* of the polarisation plane that contains information about the magnetic field component in the direction of propagation of the beam and thus allowing obtaining information about the radial profile of the current flowing in the plasma.
- *CM phase shift angle* between the two orthogonal components of the electric vector as the FIR beam becomes elliptically polarised. These measurements can be also used to recover LID.

In the first approximation, one can write these measurements in mathematical form as follows:

Interferometry phase shift

$$\varphi_{interf} \propto \lambda \int n_e dz. \tag{1}$$

Faraday rotation angle

$$\Delta\Psi = \Psi - \Psi_0 \propto \lambda^2 \int n_e B_z dz, \tag{2}$$

and Cotton-Mouton angle

$$\Phi = \varphi - \varphi_0 \propto \lambda^3 \int n_e \left(B_x^2 - B_y^2\right) dz. \tag{3}$$

Here, z is the propagation direction of the laser beam; λ is the laser wavelength; n_e is the electron plasma density; B_x, B_y, and B_z are the components of the magnetic field; Ψ_0 and φ_0 are the initial azimuth angle and phase shift; and Ψ and φ are the measured azimuth angle and phase shift during plasma at a certain time point.

B. Polarimetry methods used on JET

An optical system such as the JET FIR system contains many components such as lenses, mirrors, beam-splitters, windows, polarisers, phase retarders, isotropic, and dichroic attenuators.

The previous calibration method, based on the Stokes vector technique[15] and the Müller matrix formalism,[16] has the following limitations:

- Range of parameters limited (not very high Faraday or CM angle, for example).
- Simplify the whole optic system just to two retarders and wire grid.

As practice shown, applied procedure is time consuming and therefore not suitable for real-time plasma control.

The complex amplitude ratio calibration method on the other hand is a novel technique[17] whose methodology reduces to determination of three complex numbers by simple inversion of transfer matrix, is fast, and therefore suitable for real-time applications. The limitations to its application are mainly technical as it involves the use of complex numbers so real-time architecture has to contain packages that can perform such calculations. In addition, it must be possible to represent all polarising components in the system by a 2×2 Jones matrix (see below).

C. Polarization state description

The polarisation state of an elliptically polarised and rotated wave is schematically described in Figure 6. This state can be considered as

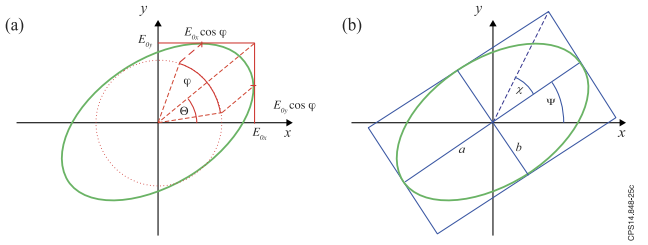

FIG. 6. Two sets of angular parameters of polarization ellipse used in polarimetry: (a) "amplitude ratio-phase difference" parameters (Θ, φ) and (b) "azimuth-ellipticity" parameters (Ψ, χ).

(a) complex electrical vector **E**,

$$\mathbf{E} = E_x\mathbf{i} + E_y\mathbf{j} = E_{0x}e^{i\varphi_x}\mathbf{i} + E_{0y}e^{i\varphi_y}\mathbf{j}, \tag{4}$$

(b) angular variables (Θ, φ):

- the auxiliary angle Θ—the ratio between the amplitudes of orthogonal components of the electrical vector,

$$\tan\Theta = \frac{|E_y|}{|E_x|} = \frac{E_{0y}}{E_{0x}}, \tag{5}$$

- the phase shift difference φ—the phase difference between two orthogonal components of the electrical vector,

$$\varphi = \varphi_y - \varphi_x, \tag{6}$$

(c) CAR defined as

$$\zeta = \frac{E_y}{E_x} = \tan\Theta \exp(i\varphi). \tag{7}$$

D. Initial polarisation state

The calibration scan contains three elements: the neutral position that is the position prior to the plasma pulse and the upper and lower limits corresponding to the expected Faraday rotation angle for that particular channel during a particular plasma experiment.

The initial polarisation state is linear ($\varphi_0 = 0$), set by the half-wave plate Θ_0. Therefore, the initial complex amplitude ratio can be calculated as

$$\zeta_0 = \tan(\Theta_0). \tag{8}$$

E. Signal detection

At JET, for each line of sight or channel, a polarisation analyser (wire grid) separates the two orthogonal components of the polarisation that are acquired by the interferometer and polarimetry detectors, called i (t) and p (t), respectively.

After analogue filtering and amplification, these signals are processed via analogue phase sensitive electronics (time constant 2–10 ms) to obtain four analogue measurements as shown,[16]

$$\begin{aligned} \mathrm{RMS} &= \langle \mathrm{i}(t) \times \mathrm{i}(t) \rangle \quad \mathrm{RMP} = \langle \mathrm{i}^*(t) \times \mathrm{i}^*(t) \rangle, \\ \mathrm{PSD} &= \langle \mathrm{i}(t) \times \mathrm{p}(t) \rangle \quad \mathrm{PSP} = \langle \mathrm{i}^*(t) \times \mathrm{p}(t) \rangle, \end{aligned} \tag{9}$$

where $\mathrm{i}^*(t)$ is $\mathrm{i}(t)$ shifted by 90° and the RMS, RMP, PSD, and PSP were defined as names for electronics modules inside a phase sensitive electronic unit.

These four signals can be represented as signal ratios called R and R' which are related to the polarisation (Θ, φ) of the detected beam,

$$\begin{cases} R = \dfrac{PSD}{RMS} = K^{-1}\tan(\Theta)\cos(\varphi) \\ R' = \dfrac{PSP}{\sqrt{RMS \cdot RMP}} = K^{-1}\tan(\Theta)\sin(\varphi) \end{cases}, \tag{10}$$

where K is a calibration factor introduced by electronic system.

This final, measured polarisation state can be expressed as the CAR as follows:

$$\zeta_m = (R + iR') = K^{-1}\zeta_d, \tag{11}$$

where ζ_d is the polarisation state of the beam at the detector system.

F. Calibration method

In the absence of the plasma, the initial polarisation state is changed between HWP and detectors by various optical components (lenses, mirrors, plates, beam splitters, and wave guides), acting as polarizers, phase retarders, isotropic, and dichroic attenuators. Such a system of objects could be modelled by the Jones matrix in the general form, derived in Ref. 18. As the local coordinate system defined by the orientation of the wire grid in front of the detectors is rotated by an unknown angle (see the Appendix) relative to the fast normal wave ellipse axis of the optical system, the Jones matrix has to be additionally multiplied by a rotation matrix. However, this operation does not alter the overall structure of the transformation matrix, which is composed of four complex elements of a Jones matrix,[17,18]

$$\mathbf{J}^{op} = \begin{bmatrix} j_{11} & j_{12} \\ j_{21} & j_{22} \end{bmatrix}. \tag{12}$$

The beam with initial polarisation $\mathbf{E}_0$ or ζ_0 set by the half-wave plate has a final polarisation given by the electric vector $\mathbf{E}_d = \mathbf{J}^{op}\mathbf{E}_0$ or the complex amplitude ratio

$$\zeta_d = \frac{E_{dy}}{E_{dy}} = \frac{j_{21}E_{0x} + j_{22}E_{0y}}{j_{21}E_{0x} + j_{22}E_{0y}} = \frac{1 + \frac{j_{22}}{j_{21}}\frac{E_{0y}}{E_{0x}}}{\frac{j_{21}}{j_{21}} + \frac{j_{22}}{j_{21}}\frac{E_{0y}}{E_{0x}}} \tag{13}$$

or

$$\zeta_d = \frac{1 + a\zeta_0}{b + c\zeta_0}. \tag{13a}$$

According to Equation (11), the final, measured polarisation state will be

$$\zeta_m = K^{-1}\zeta_d = \frac{1 + A\zeta_0}{B + C\zeta_0}, \tag{14}$$

where A = a, B = b · K, and $C = c \cdot K$.

The full characteristics of the optical and electronic systems can then be calculated in the calibration process using these three complex parameters A, B, and C.

These parameters can be determined from the measurements for n arbitrary initial polarisations, described by complex amplitude ratio ζ_{0k}, $k = 1,2,3,\ldots,n$,

$$\zeta_{mk} = \frac{1 + A\zeta_{0k}}{B + C\zeta_{0k}}. \tag{15}$$

Hence,

$$-A\zeta_{0k} + B\,\zeta_{mk} + C\zeta_{0k}\,\zeta_{mk} = 1.$$

This relation can be transformed into a system of n linear equations for three complex parameters A, B, and C,

$$\mathbf{M}\cdot\mathbf{X} = \mathbf{1},$$

where

$$\mathbf{M} = \begin{bmatrix} -\zeta_{01} & \zeta_{m1} & \zeta_{01}\zeta_{m1} \\ -\zeta_{02} & \zeta_{m2} & \zeta_{02}\zeta_{m2} \\ \vdots & \vdots & \vdots \\ -\zeta_{0n} & \zeta_{mn} & {}_{0n}\zeta_{mn} \end{bmatrix}, \mathbf{X} = \begin{bmatrix} A \\ B \\ C \end{bmatrix}, \quad \mathbf{1} = \begin{bmatrix} 1 \\ 1 \\ \vdots \\ 1 \end{bmatrix}. \tag{16}$$

The solution of Equation (16) for individual values for the unknown parameters can easily be found from matrix relation

$$\mathbf{X} = (\mathbf{M}^*\mathbf{M})^{-1}\mathbf{M}^*\mathbf{1}, \tag{17}$$

where $\mathbf{M}^*$ represents the conjugate transpose of matrix $\mathbf{M}$. Although to obtain complex parameters A, B, and C is sufficient the measurement for only three arbitrary initial polarizations ζ_{0k}, in order to increase the accuracy of the calibration procedure more measurements of the initial polarisations are recommended to be used in the iteration process.

G. Application to the plasma measurements

In the case of the beam crossing a magnetised plasma, the initial polarisation ζ_0 is changed so that at the front of the optical detection system the beam has polarisation ζ_p. Then, the final, measured polarisation state will be

$$\zeta_m = \frac{1 + A\zeta_p}{B + C\zeta_p}. \tag{18}$$

Therefore, applying the calibration parameters A, B, and C, it is possible to evaluate the polarisation state of the beam after crossing the magnetized plasma as

$$\zeta_p = \frac{1 - B\zeta_m}{-A + C\zeta_m}. \tag{19}$$

From this, one can easily recover the information on azimuth angle, ellipticity, and phase shift and amplitude ratio with the following formulas:[17]

$$\begin{aligned} &\text{Azimuth angle} && \Psi = \mathrm{Re}(\arctan\ \zeta_p), \\ &\text{Ellipticity} && \varepsilon = \tanh\left(\mathrm{Im}\ (\arctan\ \zeta_p)\right), \\ &\text{Phase shift} && \varphi = \arg(\zeta_p), \\ &\text{Amplitude ratio} && \Theta = \arctan\left|\zeta_p\right|. \end{aligned} \tag{20}$$

Relations for phase shift and amplitude ratio come from Equation (7) and relations for azimuth angle and ellipticity are derived at the Appendix.

H. Evaluation of LID measurements

In the case of JET, at least for the vertical channels, the major contribution of the magnetic field component perpendicular to the laser beam direction is the toroidal magnetic field, approximatively constant along the path. From Equation (3), it could be concluded that

$$\mathrm{LID}_{\mathrm{polarimetry}} = \int \mathrm{n_e}\,\mathrm{dz} \approx \mathrm{C_{ch}} \times \frac{\Phi}{\lambda^3 \mathrm{B_T^2}}, \tag{21}$$

where $\mathrm{C_{ch}}$ is a constant depending on the channel geometrical position within JET vacuum vessel centre.

However, in JET case, at high plasma densities and plasma currents, there is observed difference between line integrated density obtained from Equation (21) and from interferometry (Equation (1)). The discrepancy between the line-integrated density measured by polarimetry with respect to interferometry can be explained by the mutual interference between Faraday rotation and Cotton-Mouton effects[5,15,19,20] as well as the fact that perpendicular component of the measured total magnetic field is not exactly the plasma toroidal field.

To alleviate the first effect, at least in the JET case, we decided to use the LID derived from ellipticity as will be explained in Sec. IV.

The relationship between ellipticity defined as $\varepsilon = \tan(\chi)$ and azimuth Ψ and phase shift angle $\varphi = \Phi$ (as $\varphi_0 = 0$) is as follows:

$$\begin{aligned} \tan(\Phi) &= \frac{\tan(2\chi)}{\sin(2\Psi)}, \\ \tan(2\chi) &= \sin(2\Psi) \times \tan(\Phi). \end{aligned} \tag{22}$$

As can be noticed, the initial setup of 45° for azimuth angle maximises[5] the ellipticity.

Before the plasma pulse, Equation (22), therefore, becomes

$$\tan(\Phi) = \frac{\tan(2\chi)}{\sin(90)} = \tan(2\chi). \tag{23}$$

In the small Faraday angle approximation, the Cotton-Mouton angle can be measured at any magnitude as doubled ellipticity angle,

$$\Phi = 2\chi. \tag{24}$$

However, at larger Faraday rotation and Cotton-Mouton angles, this equation is not anymore valid as the Faraday angle component in Equation (22) is not negligible anymore.

On typical JET plasma with high current and high density, the Faraday rotation and Cotton-Mouton angle are larger than 10° even at small ellipticity ($\chi \ll 5°$).

As an example, for an angle variation of 15° (from the initial value of 45°), Equation (22) becomes

$$\tan(\Phi) = \frac{\tan(2\chi)}{\sin(2 \times [45 - 15])} = 1.15 \times \tan(2\chi). \tag{25}$$

As the LID varies linearly with Cotton-Mouton angle, the impact of this mutual interference on density is relevant (>10% in this example).

To resolve the mutual interaction between the two effects, one has to use a complicated mathematical apparatus of a set

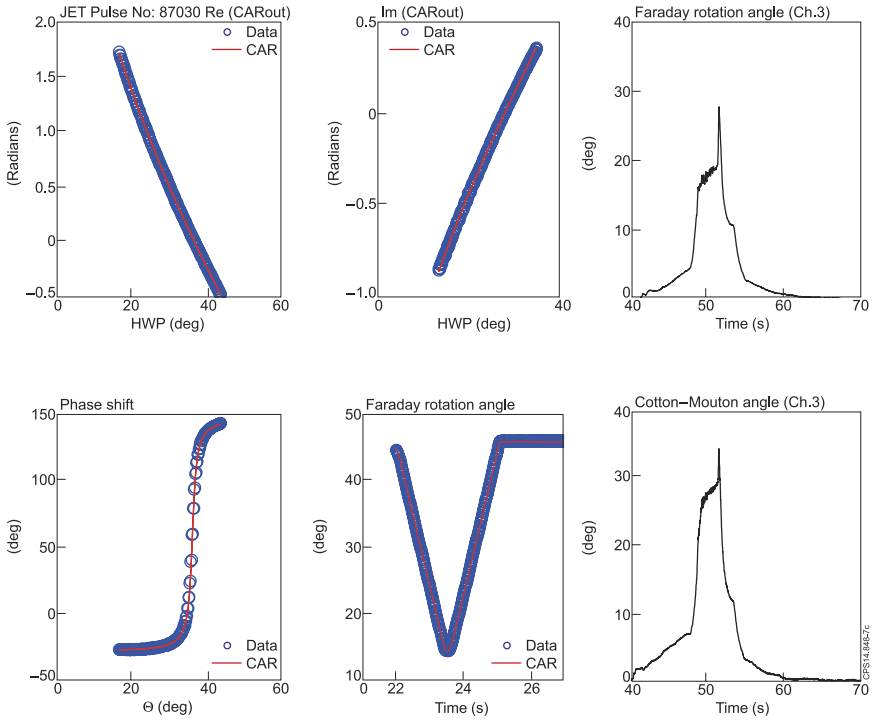

FIG. 7. ζ_m calculated (line) and measured (circles) polarisation state, Faraday rotation angle, and Cotton-Mouton phase shift during the calibration period (22-32 s) and during a JET plasma discharge (starting at 40 s) for channel 3 on pulse 87030.

of self-consistent differential equations for which the solution can be found only if both density and current profiles are known *a priori* (see Ref. 3). This is not the case for the on-line real-time calibration.

Therefore, in the JET case, for the core channel, it was found *empirically* and with the mathematical support described above, that instead of the expression in (21), a new formula for LID derived from polarimetry using ellipticity can be expressed as

$$\mathrm{LID}_{\mathrm{ellipticity}} = \int \mathrm{n_e}\, \mathrm{dz} \approx \mathrm{C_{ch}} \times \frac{2\,\chi}{\lambda^3 \mathrm{B_T^2}}. \tag{26}$$

With respect to the second reason of discrepancy between interferometry and polarimetry derived LID, due to the field structure (see Figure 13 in Section IV), this is still an open problem as we do not have the magnetics structure in real-time yet (EFIT++ being an offline program and the real-time EQUINOX package was not designed for protection systems).

IV. MEASUREMENTS

A typical example of the calibration results is shown in Figure 7.

Here, the top left pictures represent the real and imaginary parts of ζ_m, where the bottom left displays the calculated values of the phase shift and Faraday angle during the calibration period. For completeness, the Faraday rotation and Cotton-Mouton angle calculated with the CAR method during plasma pulse are also displayed on the right side of the figure.

The error level for both Faraday and Cotton-Mouton angles is 0.2° or less and has been determined statistically.

TABLE I. Calibration output for channel 3 on pulse 87030.

Calibration parameters	Real part	Imaginary part
A	1.37	−0.04
B	0.19	0.09
C	0.25	0.16
Coefficient of determination	0.9999	0.9998

The values of the calibration parameters for the pulse 87030 presented in Figure 7 as well as the quality of the fit evaluated with the coefficient of determination are shown in Table I.[21]

The measured range calibration parameters are dependent mostly on the properties of the optical system. Figure 8 is an example of the evolution of the calibration parameters *A*, *B*, and *C* for 100 consecutive pulses (one week of experimental campaign at JET). For this week, the parameter values are spread on a small bandwidth even for large variation of laser power during the operational day. It has been noticed that this has a small impact on Faraday rotation angle measurements but it has some impact to the signal to noise ratio (SNR) of the evaluated density based on polarimetry and sometime the error level in term of density is larger than one fringe (1 fringe equals with 1.143×10^{19} particles/m^2).

The new method is very robust even when the laser signal level is 30 dB lower than nominal value and is operational on all eight channels as displayed in Figure 9.

The measurements of the new real-time system are very similar to the CAMAC-based counterpart but with better resolution due to the lower bit noise of the PowerPC system. An example of this comparison is given in Figure 10 that

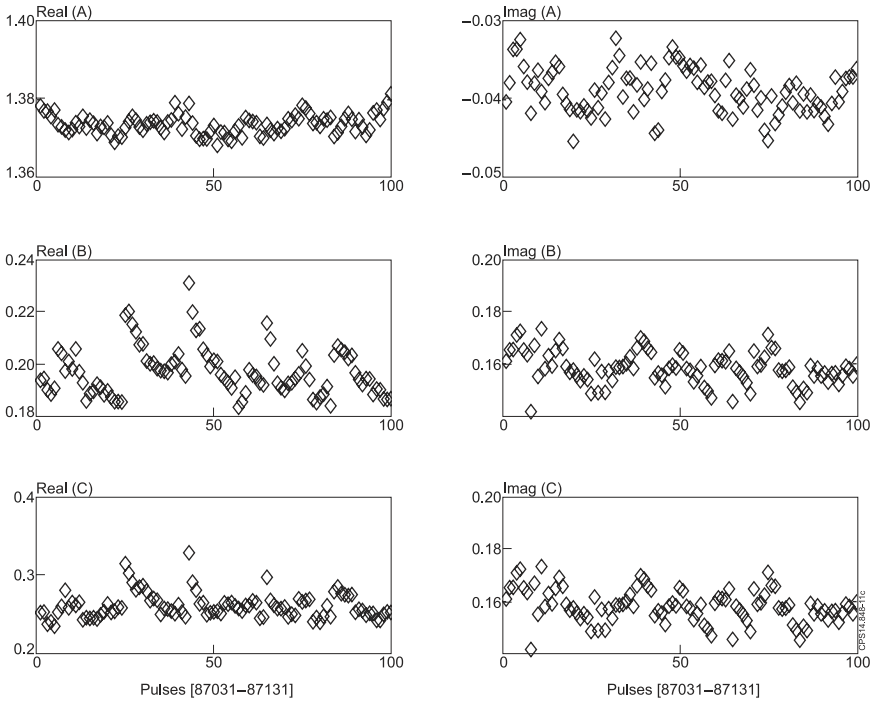

FIG. 8. Evolution of calibration parameters for 100 consecutive plasma pulses during the 2014 JET campaign.

contains the calculated Faraday rotation angle for the vertical channels for all recorded data including calibration time.

The method was tested extensively and with particular attention to high performance plasmas with high current during which the Faraday angle and Cotton-Mouton phase shift are large (>15°).

An example is displayed in Figure 11 for a pulse with 3.5 MA plasma current and more than 20 MW additional heating power. In this pulse, the maximum Faraday angle is greater than 20° and the Cotton-Mouton angle more than 30° whilst the line-integrated density has a value of 20 fringes (again 1 fringe equals with 1.143×10^{19} particles/m^2).

Note: on JET, the convention is that the time zero corresponds to the start of plasma current so from now the time axis starting with zero refers only for data during plasma pulse and does not contain the polarimetry calibration period.

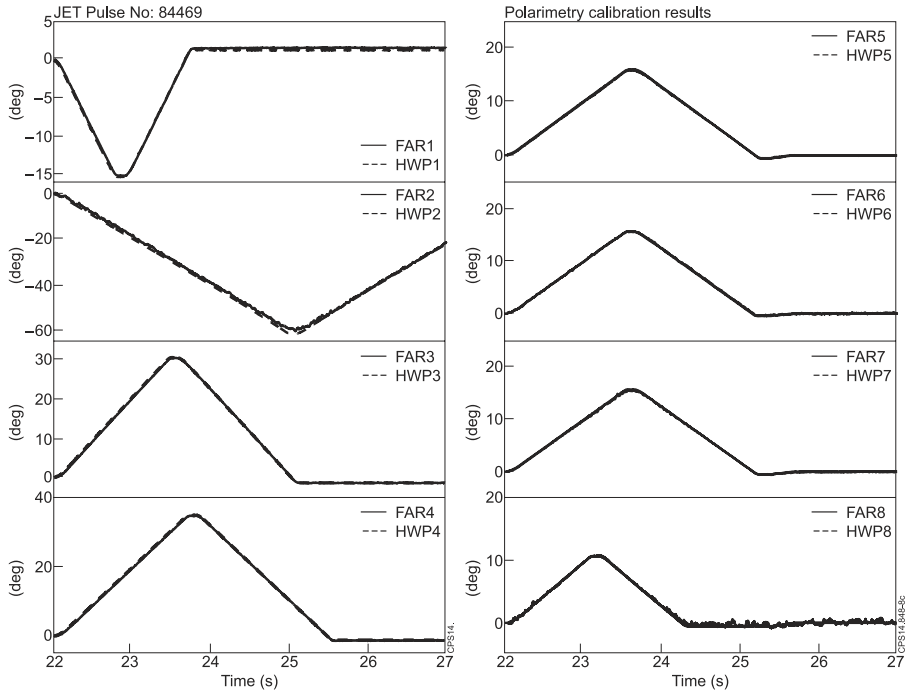

FIG. 9. Calibration output for all 8 channels. HWP and FAR represent the mechanical position of the half-wave plate and the calculated Faraday rotation angle from the detected laser signals.

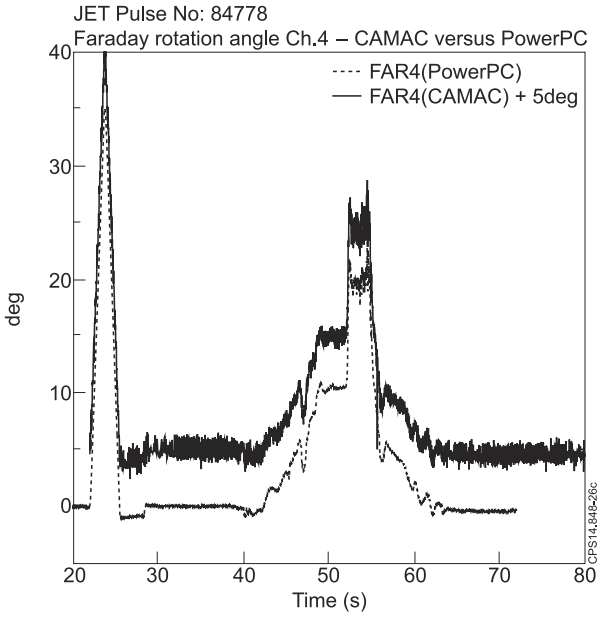

FIG. 10. Measured Faraday rotation angles for the vertical channels during pulse 84778—solid lines are measurements from the new PowerPC-based system and dashed lines from the old CAMAC-based system.

V. INTEGRATION OF POLARIMETRY INTO MACHINE PROTECTION

A. Preamble

The current JET machine has measurements of the LID provided by interferometer, hard wired into the density feedback system and the interlock system of additional heating by neutral beams injection (NBI). With the installation of the new ITER-like metallic wall of the vacuum vessel, advanced plasma scenarios and new effects such as tungsten impurity influx into plasma put the interferometer signal at risk. The interferometer's major weakness is that it is a history-dependent measurement (within the pulse) and any loss of signal for long enough time intervals will invalidate the measurement for the rest of the discharge. In the past, JET relied on a backup of density provided by bremsstrahlung radiation measurements but in the ITER-like wall this measurement is deemed not safe for NBI protection due to potential contamination by tungsten line radiation.

B. Plasma density validation on JET

After a detailed validation phase, JET now operates with the line-integrated density from polarimetry as a backup measurement to the one provided by interferometry. In Figure 12 is depicted the flow-logic of the PDV at JET. Every signal within PDV has an equivalent validity flag and the signals are activated in a cascade manner (ranks). The logic is kept simple; when one signal is not deemed valid, the PDV skips to next signal and so on.

The LID measurement from polarimetry has some limitations as shown:

- Mutual interference between Faraday and Cotton-Mouton effects is very strong at high density.
- 10 ms delay in data provision due to the integration time of electronics.
- The change of toroidal magnetic field caused by plasma diamagnetic effects[22] is not taken into account.
- Radial and poloidal magnetic fields' contribution to total magnetic field not readily available in real-time as to obtain this information one has to compute a very complex magnetic field structure software inversion.

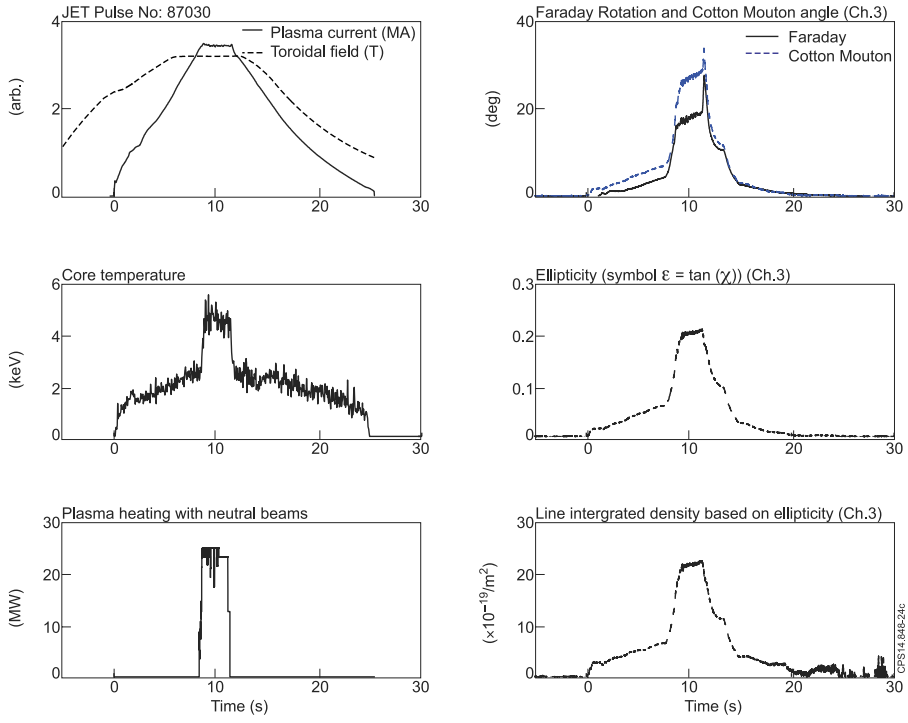

FIG. 11. Various plasma parameters and polarimetry measurements for the high current plasma pulse 87030.

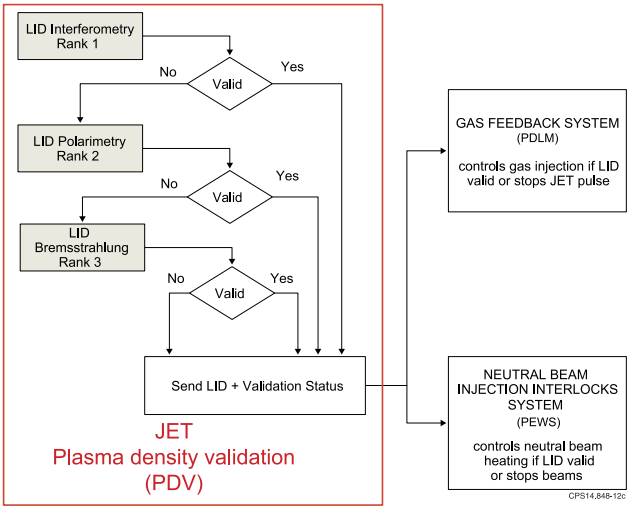

FIG. 12. Plasma Density Validation (PDV) and links with various protection systems.

C. Polarimetry versus interferometry for plasma density control

An example of the reconstruction of LID from ellipticity using the approximation given in Equation (26) is shown in Figure 13. In this figure, the use of the vacuum toroidal magnetic field is compared to evaluating Equation (26) using *a posteriori* the toroidal field calculated from an equilibrium reconstruction for this discharge (EFIT++/B_t). One can see in the top left panel of Figure 13 that the equilibrium toroidal field can vary by about 1% from the vacuum field. This can generate an error in the calculated LID of 2%. This is an important source of error at low density and low Faraday angle (bottom right panel of Figure 13). During the high density phase (7-12 s in this example), on the other hand, the dominant error is due to the interaction between the Faraday rotation and the Cotton-Mouton effect. For the vertical line-of-sight shown in Figure 13, the correction due to radial field is expected to be small as its magnitude is only about 2% of the toroidal field (bottom left panel of Figure 13) and it enters via the Cotton-Mouton effect only as $(B_t^2 - B_r^2)$ (Equation (3)). Corrections due to the vertical field (bottom left panel of Figure 13) enter via the Faraday rotation (Equation (2)) and are expected to be small at low Faraday angles.

It is worth mentioning that the original polarimeter design was on the assumption that there is no mutual interaction between Faraday rotation and Cotton-Mouton effects.

We alleviated these effects by evaluating line-integrated electron density from ellipticity (see Equation (26)) and not Cotton-Mouton phase shift angle and by scaling (division) the measured density from polarimetry in order to ensure that the new measurement *always underestimates* the actual density (measured normally by the interferometer) by a certain value so polarimetry errors are the side of caution from the JET machine protection point of view. The implementation of the new measurements was following a very strict set of rules and involved several software iterations and parallel checks. The current scaling factor has been set to the value 1.2 using a very conservative approach (ref. pulse 87030). The current value range will be revised based on experience that will be acquired in the next campaigns.

The new method of calibration proved to be very robust for the JET configuration even if the system is not optimised

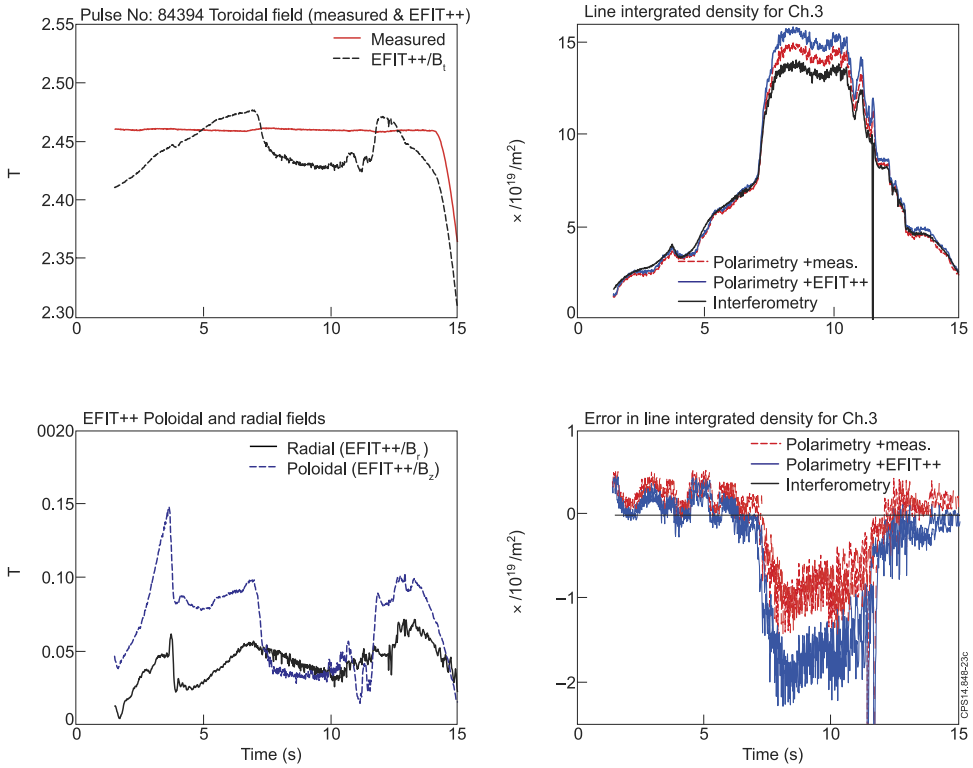

FIG. 13. Line-integrated magnetic field components normal to propagation direction of channel 3 of polarimetry and calculated line integrated densities using ellipticity and toroidal field and EFIT components.

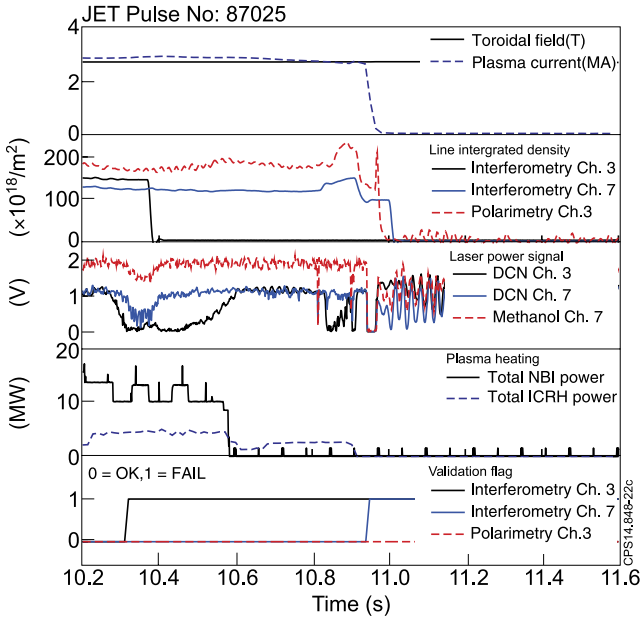

FIG. 14. Example of various line-integrated density (LID) measurements used for machine protection at JET (interferometry ch 3 and 7 and polarimetry ch 3, signal makers for laser power of DCN, and methanol lasers as well as validity flag).

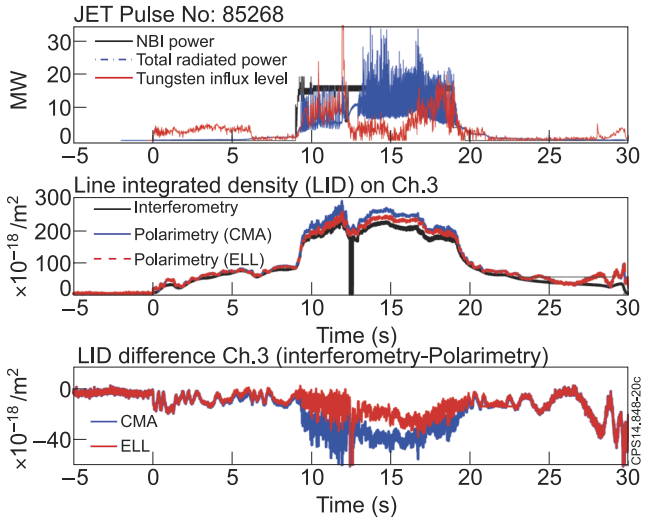

FIG. 15. Line-integrated density for a pulse that is affected by tungsten impurity influx.

for the best signal to noise ratio. However, it was observed that the laser power has a strong impact on the line-integrated electron density measurements from polarimetry as the error level in this case can be larger than one fringe. This becomes critical when this measurement is used actively for plasma gas feedback control and protection systems so further instrumentation is being added to monitor better the lasers.

Figure 14 shows a typical example of the evolution of the density control in the case of a pulse with a tungsten impurity influx. In this particular case, the control of density switched to one of the interferometer lateral channels after the main vertical channel of interferometry fails as early as about 10.4 s from plasma start (signal level for core drops to zero, third plot from the top). This signal level represents the minimum voltage peak-to-peak of 100 samples (acquired every 10 μs) and processed internally. If any of these signals drops below a low threshold voltage (90 mV), the signal is deemed lost. Here relies the main weakness of the interferometry: one single lost sample will set the interferometer signal bad as phase measurement is history dependent. Polarimetry, on the other hand, provides an absolute measurement and due to longer integration time is more reliable. In contrast to interferometry, polarimetry validation error flag remains zero for the entire length of the pulse (see bottom plot in Fig. 14).

A similar example is given in Figure 15 where one can also notice that the plasma is heavily affected by these tungsten impurity events and level of radiation is very high. The LID from interferometry was reconstructed offline but there is a time interval when the density was deemed not valid and was set to zero.

Another point shown by this picture that can be noticed is the quantitative discrepancy between LID derived from ellipticity and Cotton-Mouton angle with respect to interferometry (third plot). As the difference between the LID from interferometry and polarimetry is larger for plasmas with high neutral beam power (NBI) (>15 MW), high plasma currents, and high magnetic field, several statistical analyses were done to get a better estimation of the density in the view of use for machine protection and control. One such example is displayed in Figures 16 and 17 for an entire experimental session (13 pulses). One can notice a LID difference of around 10% that does not depend on the magnitude of additional heating power at least for beam power larger by 10 MW (see second plot in Figure 17). The reason for this difference can be partially explained by the fact that the formula evaluating the line-integrated density from polarimetry does not include the radial and poloidal components of the total magnetic field as shown in Figure 13. There is also a second order correction required due to the mutual interaction of the Faraday rotation angle and Cotton-Mouton phase shift angle not fully mitigated by the use of the ellipticity in evaluating the LID. In this particular case, a scaling factor of 1.2 (division of LID from polarimetry by 1.2) will bring this measurements on the safe

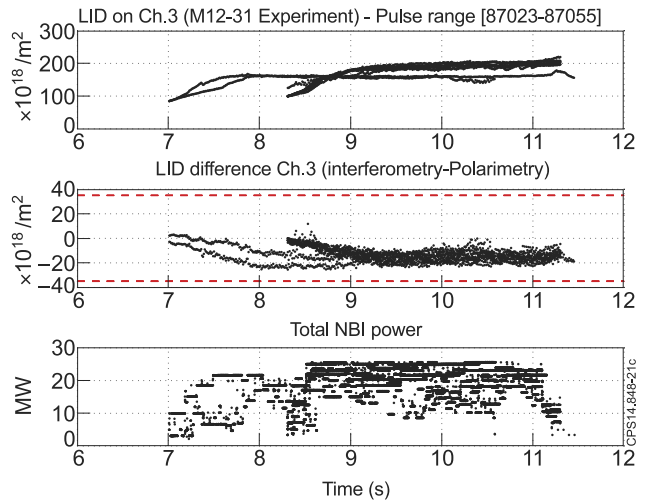

FIG. 16. Time evolution of the line-integrated density difference between interferometry and polarimetry for pulses form an entire experimental session.

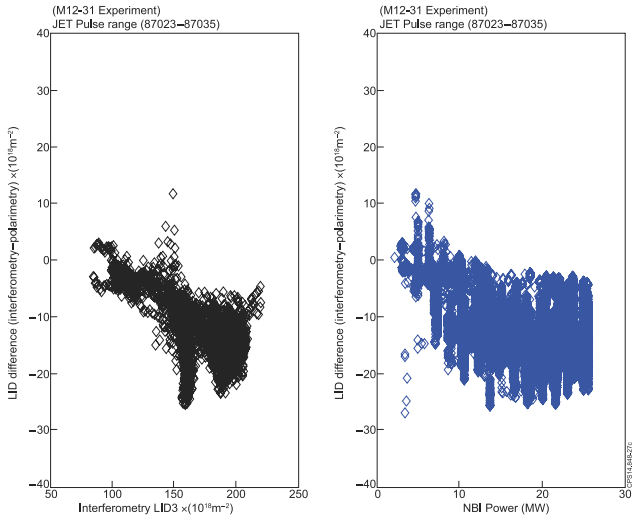

FIG. 17. The line-integrated density difference in versus absolute line integrated density as measured by the interferometry and in NBI power space.

side for use for machine protection that requires that the difference between measurements has to be in the range of 3 fringes ($\sim 3 \times 10^{19}/\mathrm{m}^2$).

D. Use of polarimetry plasma density control

The JET machine is a nuclear facility and any change of control requires extensive testing and fault simulation. Many offline tests were done by injecting previously recorded analogue data into the real-time crate PowerPC to simulate fault conditions and validation flag analysis. Following these tests, in August 2014, the Machine Protection Working Group approved the use of the LID signal from polarimetry for real time control of both gas feedback and machine protection systems (NBI interlock).

In accordance with our knowledge, this is the first time in the word that polarimetry has been used unattended for plasma control and protection of the machine as a standard routine, in the case when Faraday rotation and Cotton-Mouton effect are strong and consubstantial (in ITER relevant conditions). In Textor-94 machine, polarimetric feedback control of electron density[23] was based on Faraday rotation only, for plasma with lower electron density and plasma current, where coupling between Faraday and Cotton-Mouton effect is irrelevant and could be omitted in the analysis. A special case is the Stellarators[24,25] where LID can be measured from Cotton-Mouton measurements as the Faraday angle is very small.

This measurement proved to be 100% reliable from the first day.

In Figure 18, there is such an example. Top figure displays various LIDs used for machine protection and gas feedback control, figure two the validation flags for interferometry and polarimetry, respectively, third plot displays NBI and ion cyclotron resonance heating (ICRH) power, fourth plot the difference between interferometry and polarimetry LID, and bottom plot depicts the toroidal field and plasma current.

In this pulse, with low plasma density, there was an injection of 3 mm diameter pellets that penetrated the core causing a density increase of 80% in a few milliseconds.

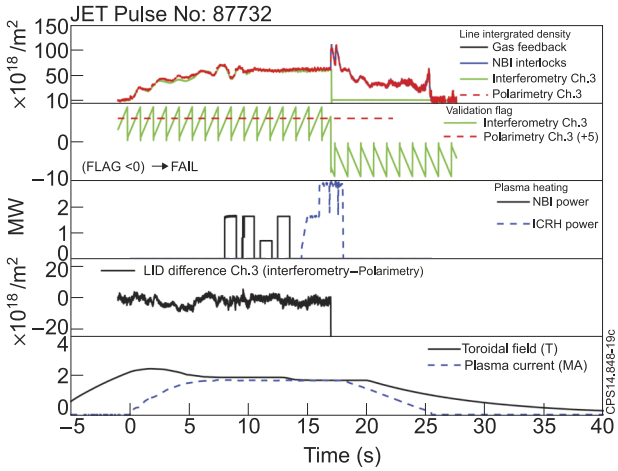

FIG. 18. Example of a pulse when LID from polarimetry was actively used for controlling gas feedback control and NBI protection during a JET plasma pulse.

The current interferometry implementation for LID detects a fault (LID3 validation flag becomes negative in the second figure) and the PDV switches safely to polarimetry LID that is still valid (the corresponding flag stays positive) and carries on for the rest of the pulse.

The difference between interferometry and polarimetry LID when both are valid is below the limit of $\pm 20 \times 10^{18}/\mathrm{m}^2$ as displayed in the third plot.

VI. CONCLUSIONS

A fast and reliable automatic polarimetry calibration based on the complex amplitude ratio method has been implemented at JET in order to provide measurements of Faraday rotation angle and line-integrated density measurements in real-time with 1 ms time resolution. The new measurements are integrated with the new offline magnetic reconstruction code EFIT++ but more important, the measurements of the LID from polarimetry are also integrated with JET plasma control and machine protection systems.

The polarimeter, with this new addition, will become an essential diagnostic for the JET experiment for the following campaign and, in particular, the D-T campaign which is a very important step for ITER developments.

This new diagnostic implementation is expected to have a great impact not only on the design of the new polarimeters envisaged for other machines (ITER, JT60SA, for example) but also on their application as this type of diagnostic could acquire elevated importance for density control and as a safety feature for plasma experiments.

VII. FURTHER DEVELOPMENTS

We are envisaging new developments in several areas: data acquisition hardware upgrade (central processing unit (CPU) upgrade), better magnetic structure information to the polarimeter (radial field information for example), and a new design of the half-wave plate assembly that can be removed/serviced via remote-handling (essential during D-T operation).

ACKNOWLEDGMENTS

We would like to thank to all our colleagues at CCFE and EU associations for this work, in particular, to M. Kempenaars and E. Zilli for careful reading and suggestions but also to A. Murari, M. Brombin, M. Gelfusa, F. Orsitto, P. Gaudio, M. Maslov, and S. Dudley for the previous work they have done in this field over recent years.

This work has been carried out within the framework of the Contract for the Operation of the JET Facilities and has received funding from the European Union's Horizon 2020 research and innovation programme. The views and opinions expressed herein do not necessarily reflect those of the European Commission.

APPENDIX: FEW WORDS ON POLARISATION AND REFERENCE SYSTEMS

The polarization ellipse shown in Figure 6 is the ellipse with the major half-axis a and the minor half-axis b, rotated by some azimuth angle Ψ. The polarization ellipse with $\Psi = 0$ is represented by a complex vector $\mathbf{E}_0 = (a, ib)$. The complex vector for the ellipse with azimuth angle Ψ, obtained by a rotation of a reference frame on angle $-\Psi$, has a form

$$\mathbf{E} = \begin{pmatrix} \cos(\Psi) & -\sin(\Psi) \\ \sin(\Psi) & \cos(\Psi) \end{pmatrix} \mathbf{E}_0 = \begin{pmatrix} a\cos(\Psi) - ib\sin(\Psi) \\ a\sin(\Psi) + ib\cos(\Psi) \end{pmatrix}. \tag{A1}$$

As a result, the complex amplitude ratio $\zeta = E_y/E_x$ takes the form

$$\zeta = \frac{a\sin(\Psi) + ib\cos(\Psi)}{a\cos(\Psi) - ib\sin(\Psi)}. \tag{A2}$$

Dividing numerator and denominator by $a\cos(\Psi)$ and taking into account that the ratio of the minor and the major half-axis is equal to the ellipticity ε or to the tangent of the ellipticity angle χ

$$\varepsilon = \tan(\chi) = \frac{b}{a}, \tag{A3}$$

the complex amplitude ratio could be written as

$$\zeta = \frac{\tan(\Psi) + i\tan(\chi)}{1 - i\tan(\Psi)\tan(\chi)}. \tag{A4}$$

In the same time, ζ could be presented as a tangent of the complex polarization angle γ[26]

$$\zeta = \tan(\gamma) = \tan(\mathrm{Re}(\gamma) + i\,\mathrm{Im}(\gamma)). \tag{A5}$$

Expressing the complex tangent functions in terms of the real and imaginary parts of its arguments

$$\tan(\gamma) = \frac{\tan(\mathrm{Re}(\gamma)) + \tan(i\,\mathrm{Im}(\gamma))}{1 - \tan(\mathrm{Re}(\gamma))\tan(i\,\mathrm{Im}(\gamma))} = \frac{\tan(\mathrm{Re}(\gamma)) + i\tanh(\mathrm{Im}(\gamma))}{1 - i\tan(\mathrm{Re}(\gamma))\tanh(\mathrm{Im}(\gamma))} \tag{A6}$$

and comparing with Equation (A4), we conclude that $\tan(\mathrm{Re}(\gamma)) = \tan(\Psi)$ and $\tanh(\mathrm{Im}(\gamma)) = \tan(\chi)$. Thus, azimuthal angle Ψ coincides to the real part of the inverse tangent of the complex amplitude ratio

$$\Psi = \mathrm{Re}(\gamma) = \mathrm{Re}(\arctan(\zeta)). \tag{A7}$$

Whereas ellipticity equals

$$\varepsilon = \tan(\chi) = \tanh(\mathrm{Im}(\arctan(\zeta))). \tag{A8}$$

1. Reference system for JET polarimeter

The two reference frames of the polarimeter corresponding to the half-wave plate and wire grid analyser have both as a reference the cross section plane that go in middle of the octant 7 of the JET machine. This plane is perpendicular to the entire row of half-wave plates as well as the analyser wire grids back in the lab with a tolerance of few degrees. The toroidal field direction is also perpendicular to this cross section plane.

However, the wire grids are not aligned such that the initial linear polarisation is perpendicular to the wires' direction of the wire grids' analysers due to several hardware limitations, the more important being the impact on interferometer diagnostic: at very large Faraday rotation angles (up to 70° on JET), the signal corresponding to the interferometer i(t) decreases below an acceptable threshold so the system has to be set in such a way that the values of i(t) and p(t) do not exceed a certain range during both calibration scan and actual plasma measurement.

[1]G. Braithwaite *et al.*, Rev. Sci. Instrum. **60**, 2825 (1989).
[2]D. Veron, "Submillimeter interferometry of high-density plasmas," in *Infrared and Millimeter Waves* (Academic Press, 1979), Vol. 2, pp. 67–135.
[3]S. E. Segre, Plasma Phys. Controlled Fusion **41**, R57 (1999).
[4]A. Boboc *et al.*, Rev. Sci. Instrum. **77**, 10F324 (2006).
[5]K. Guenther and JET-EFDA Contributors, Plasma Phys. Controlled Fusion **46**, 1423 (2004).
[6]A. Boboc *et al.*, in *IRMMW-THz. Conference* (IEEE, 2007), Vol. 1, p. 378.
[7]B. Alper *et al.*, in 37th EPS Conference, P2.173.
[8]See http://en.wikipedia.org/wiki/Computer_Automated_Measurement_and_Control for extended information about CAMAC architecture.
[9]See http://en.wikipedia.org/wiki/PowerPC for extended information about PPC architecture.
[10]Yu. A. Kravtsov and B. Bieg, J. Plasma Phys. **76**, 795–807 (2010).
[11]D. Mazon *et al.*, Plasma Phys. Controlled Fusion **45**, L47 (2003).
[12]See http://en.wikipedia.org/wiki/Field-programmable_gate_array for extended information about FPGA architecture.
[13]F. Bombi *et al.*, IEEE Trans. Nucl. Sci. **25**, 243 (1978).
[14]L. C. Appel *et al.*, "A unified approach to equilibrium reconstruction," in *33rd EPS Conference on Plasma Physics* (EPS, Rome, Italy, 2006), p. 2.184.
[15]F. P. Orsitto *et al.*, Plasma Phys. Controlled Fusion **50**, 115009 (2008).
[16]M. Gelfusa *et al.*, Rev. Sci. Instrum. **81**, 053507 (2010).
[17]B. Bieg *et al.*, Fusion Eng. Des. **88**, 1452 (2013).
[18]I. Scierski and F. Ratajczyk, Optik **68**, 121 (1984).
[19]F. P. Orsitto *et al.*, Rev. Sci. Instrum. **81**, 10D533 (2010).
[20]S. E. Segre, Plasma Phys. Controlled Fusion **35**, 1261 (1993).
[21]See http://en.wikipedia.org/wiki/Coefficient_of_determination for definition, use, and additional information.
[22]V. D. Shafranov, Plasma Phys. **13**, 757 (1971).
[23]H. R. Koslowski *et al.*, in *Proceedings of the SOFT* (Elsevier, Lisbon, 1996), p. 845.
[24]Ch. Fuchs and H. J. Hartfuß, Rev. Sci. Instrum. **70**, 722 (1999).
[25]Ch. Fuchs and H. J. Hartfuß, Phys. Rev. Lett. **81**, 1626 (1998).
[26]Z. H. Czyz *et al.*, Phys. Lett. A **368**, 101 (2007).
[27]Full documentation of CODAS electronics and infrastructure (as CTTS and RTDN, for example) is managed through internal JET Document Notes (JDN) documentation that is not freely available but could be provided on request.